Role of the thermal $f_0(500)$ in chiral symmetry restoration

S. Ferreres-Solé,[1,*] A. Gómez Nicola,[2,†] and A. Vioque-Rodríguez[2,‡]
[1]NIKHEF, Science Park 105, NL-1098 XG, Amsterdam, Netherlands
[2]Departamento de Física Teórica and IPARCOS. Univ. Complutense., 28040 Madrid, Spain

(Received 24 November 2018; published 26 February 2019)

We show that the $\sigma/f_0(500)$ state with finite-temperature T corrections to its spectral properties included plays an essential role for the description of the scalar susceptibility χ_S, signaling chiral symmetry restoration. First, we use the $O(4)$ linear sigma model as a test bed to derive the connection between χ_S and the σ propagator and to check the validity and reliability of the approach where χ_S is saturated by the $\sigma/f_0(500)$ inverse self-energy, which we calculate at finite T to one loop. A more accurate phenomenological description is achieved by considering the saturation approach as given by the thermal $f_0(500)$ state generated in unitarized chiral perturbation theory (UChPT). Such an approach allows us to describe fairly well recent lattice data within the uncertainty range given by the UChPT parameters. Finally, we compare the UChPT saturated description with one based on the hadron resonance gas, for which the hadron mass dependences are extracted from recent theoretical analysis. Several fits to lattice data are performed and confirm the validity of the thermal $f_0(500)$ saturated approach and hence the importance of that thermal state for chiral symmetry restoration.

DOI: 10.1103/PhysRevD.99.036018

I. INTRODUCTION

Chiral symmetry restoration and its nature are surely among the key problems for our present understanding of the QCD phase diagram. It is well established that in the physical case of $N_f = 2 + 1$ flavors with $m_l \ll m_s$ quark masses the chiral transition is a crossover at a transition temperature of about $T_c \sim 155$–160 MeV for vanishing baryon density [1–4]. The ideal chiral restoration phase transition is reached only for $N_f = 2$ and $m_l = 0$, while in the physical case, it is approached in the light chiral limit $m_l \to 0^+$ [5].

The main signals of a chiral restoration crossover are, on the one hand, the decreasing behavior of the quark condensate $\langle \bar{q}q \rangle_l = \langle \bar{\psi}_l \psi_l \rangle$, where $\psi_l = \binom{u}{d}$ is the light quark doublet, and, on the other hand, a peak in the scalar susceptibility $\chi_S(T)$, where

$$\langle \bar{q}q \rangle_l(T) = \partial z(T)/\partial m_l, \tag{1}$$

$$\chi_S(T) = -\frac{\partial}{\partial m_l} \langle \bar{q}q \rangle_l(T) = \int_T d^4x [\langle \mathcal{T}(\bar{\psi}_l \psi_l(x) \bar{\psi}_l \psi_l(0)) \rangle - \langle \bar{q}q \rangle_l^2(T)], \tag{2}$$

$\int_T dx \equiv \int_0^\beta d\tau \int d^3\vec{x}$ at finite temperature $T = 1/\beta$, we are considering the isospin limit $m_u = m_d = m_l$, and $\langle \cdot \rangle$ denotes Euclidean finite-T correlators. The free energy density in the above equations is $z(T) = -\lim_{V\to\infty}(\beta V)^{-1} \log Z$ at finite temperature T with vanishing chemical potentials, with Z the QCD partition function or its hadronic realization through an effective theory. Thus, the scalar susceptibility χ_S in (2) should peak at the chiral transition or diverge in the light chiral limit for $N_f = 2$ [6,7], and this is indeed reflected in lattice data [1] in which the peak of χ_S confirms the crossover nature of the transition in the physical limit.

From the theoretical side, it is important to provide reliable approximations which could describe the expected behavior for the quark condensate and the scalar susceptibility and eventually be used to fit lattice data. The most widely used approach in this context has been the hadron resonance gas (HRG) approximation [8–15]. Within the HRG, the pressure of the system is described as a collection of free resonances, including in principle all hadron states quoted by the Particle Data Group (PDG) [16] up to a given energy above which Boltzmann suppression is effective. Thus, hadron interactions are meant to be encoded through their corresponding resonant channels, and the width of the resonant states is usually neglected. This approximation

*ferreres.sole@gmail.com
†gomez@ucm.es
‡avioque@ucm.es

works quite well below T_c, where it is meant to be valid, although qualitatively it does not reproduce the inflection point expected for the quark condensate nor, as we will see in detail here, the peak of the scalar susceptibility in the crossover regime.

Calculations of the thermodynamics including interactions among hadrons encompass the chiral perturbation theory (ChPT) description of the light meson gas [17], which provides a model-independent and consistent treatment. Although restricted to low temperatures, it captures well the contribution of the lightest states. An alternative is the virial approach, in which interactions are incorporated within a small fugacity expansion. Both ChPT and the virial approach predict similar results consistent with chiral symmetry restoration [18], although higher-order states are needed, as provided by the HRG, to obtain results compatible with the lattice.

A relevant issue, not often considered, is the importance of the interactions among the thermal bath components, which ultimately give rise to a temperature dependence of the hadron spectral parameters (mass and width, generally speaking). As a particular example of relevance for the present work, the ChPT analysis of pion scattering at finite temperature combined with unitarity arguments [19,20] allows us to obtain the temperature dependence of the $\rho(770)$ and $f_0(500)$ poles in the second Riemann sheet (2RS). In the ρ case, the results are compatible with the observed widening in the dilepton spectrum, parametrized through the pion form factor [21], but the more important consequence for our present work concerns the $f_0(500)$ channel, since the analysis in Ref. [22] shows that the scalar susceptibility saturated by such thermal $f_0(500)$ state has a maximum very close to the expected transition point, which is quite remarkable given the approximations used.

In this work, we will explore in detail some phenomenological and theoretical aspects related to the scalar susceptibility description through the $f_0(500)$ thermal state. Our aim and motivation are to investigate to what extent the thermal $f_0(500)$ must be taken into account when describing observables regarding the chiral transition. The scalar susceptibility is the candidate for which the influence of such a state is meant to be dominant, since, as we will explain below in detail, it should scale roughly as the inverse thermal mass squared of the scalar propagator, for which the $f_0(500)$ gives the lightest contribution.

Our analysis will proceed along the following lines. The formal connection of the $f_0(500)$ with the scalar susceptibility will be discussed in Sec. II, in which we will focus the discussion on the $O(4)$ linear sigma model (LSM) as an example of a theory including explicitly the σ degree of freedom, in which the connection between the scalar susceptibility and the σ self-energy will be analyzed, and on unitarized ChPT (UChPT), which provides a more accurate description of the $f_0(500)$ state at $T = 0$ without the need of such a state in the Lagrangian. In both cases, we will see that the saturated approach provides a description closer to lattice data, the UChPT approach reproducing the expected crossover peak unlike the LSM one. Our next step (Sec. II B) will be to check the robustness of the unitarized saturation approach and its capability to describe lattice data without further approximations. For that purpose, we will study the sensibility of the model to the uncertainties in the low-energy constants (LECs) of ChPT and to the requirements imposed by the unitarization method, such as unitarity, analiticity, and a good determination of the $T = 0$ pole. In Sec. III, we will present a HRG analysis of the scalar susceptibility, which as far as we know has not been studied so far. Finally, in Sec. IV, we will perform detailed fits of lattice data to the unitarized model, comparing it with the HRG description. Our main conclusions are summarized in Sec. V.

The present analysis will confirm the importance of considering thermal (or generally in-medium) interactions to describe certain hadron gas observables and the relevance in particular of the $f_0(500)$ thermal sate, opening up interesting possibilities for future theoretical and lattice studies.

II. THERMAL $\sigma/f_0(500)$ AND THE SCALAR SUSCEPTIBILITY

In this section, we will discuss the connection of the scalar susceptibility, defined in (2), with the lightest scalar meson state, the σ or $f_0(500)$, which is indexed in the Particle Data Book as a broad resonance arising dominantly in $\pi\pi$ scattering [16]. The $f_0(500)$ and its main properties have been recently reviewed in Ref. [23]. This connection will be studied first within the framework of the LSM as a test bed which will allow us to check the different approximations used. Second, within UChPT, we will consider a saturated approach in terms of the thermal $f_0(500)$ generated as a pole in $\pi\pi$ scattering.

A. Linear sigma model description

First, for clarifying purposes, let us consider a meson field theory realization of low-energy QCD in which there is an explicit realization of the scalar σ as a fundamental field in the Lagrangian. A particular example is the LSM or $O(4)$ vector model [24], which exhibits chiral symmetry restoration properties [25,26]. For our present discussion, it will be enough to consider the light meson sector Lagrangian of this model in terms of sigma σ and pion π^a fields,

$$\mathcal{L}_{\mathrm{LSM}} = \frac{1}{2}\partial_\mu \Phi^T \partial^\mu \Phi - \frac{\lambda}{4}[\Phi^T\Phi - v_0^2]^2 + h\sigma, \qquad (3)$$

with $\Phi^T = (\sigma, \vec{\pi})$, and we have chosen, as usual, the σ direction to break the symmetry $O(4) \to O(3)$. The h term breaks explicitly the chiral symmetry, with h proportional to the pion mass squared, whereas the potential minima at $\Phi^2 = v^2 \neq 0$ implement spontaneous chiral symmetry breaking.

For $h = 0$, $v = v_0$ (chiral limit), whereas for $h \neq 0$, the value of v is determined by the minimum of the potential $V(\sigma)$ as

$$h = \lambda v(v^2 - v_0^2). \tag{4}$$

The $T = 0$ standard procedure is to shift the field as $\tilde{\sigma} = \sigma - v$, so that $\langle\tilde{\sigma}\rangle = 0$ to leading order. At $T \neq 0$, however, $\langle\sigma\rangle(T) \equiv v(T) \neq v$, so if one decides to use the same shifted $\tilde{\sigma}$ field, as done, for instance, in Ref. [26], it should be taken into account that $\langle\tilde{\sigma}\rangle(T) = v(T) - v \neq 0$, which in particular implies that one-particle reducible (1PR) diagrams enter in the calculation of correlators, as in the case of the $\tilde{\sigma}$ propagator. An alternative, followed in Ref. [25], is to use instead the shifted field $\hat{\sigma} = \sigma - v(T)$ so that $\langle\hat{\sigma}\rangle = 0$. The temperature dependence of $v(T)$ can be determined within the LSM, for instance, from the mean-field approach to leading order in λ [25].

With the first prescription, the Lagrangian (3) becomes, in terms of the shifted $\tilde{\sigma}$ field,

$$\begin{aligned}\mathcal{L}_{\rm LSM} = &\frac{1}{2}(\partial_\mu\tilde{\sigma}\partial^\mu\tilde{\sigma} + \partial_\mu\pi^a\partial^\mu\pi^a - M_{0\sigma}^2\tilde{\sigma}^2 - M_{0\pi}^2\pi_a\pi^a)\\ &-\frac{\lambda}{4}(\tilde{\sigma}^2 + \pi_a\pi^a)^2 - \lambda v\tilde{\sigma}(\tilde{\sigma}^2 + \pi_a\pi^a)\\ &-\frac{1}{4\lambda}M_{0\pi}^4 + v^2M_{0\pi}^2,\end{aligned} \tag{5}$$

where $M_{0\pi}$ and $M_{0\sigma}$ are the tree-level pion and sigma masses

$$M_{0\pi}^2 = \frac{h}{v} = \lambda(v^2 - v_0^2), \qquad M_{0\sigma}^2 = M_{0\pi}^2 + 2\lambda v^2, \tag{6}$$

and where, in order to comply with low-energy theorems, or ChPT to leading order [27] [$\lambda \to \infty$, $\Phi^T\Phi = v_0^2$ in (3)], we have $v_0 = F$, the pion decay constant in the chiral limit, so that $v = v_0(1 + \mathcal{O}(M_\pi^2/M_\sigma^2)) = F(1 + \mathcal{O}(M_\pi^2/M_\sigma^2)) = F_\pi(1 + \mathcal{O}(M_\pi^2/M_\sigma^2))$ with $F_\pi \simeq 92.3$ MeV. In addition, we write as is customary $M_{0\pi}^2 = 2B_0 m_l$ so that to leading order in the chiral low-energy expansion, the Gell-Mann-Oakes-Renner relation $\langle\bar{q}q\rangle_l(T = 0) = -2B_0F^2(1 + \mathcal{O}(M_\pi^2/M_\sigma^2))$ holds.

Thus, the quark condensate (1) and the scalar susceptibility (2) of the LSM can be written as follows:

$$\langle\bar{q}q\rangle_l(T) = -\frac{dh}{dm_l}v(T), \tag{7}$$

$$\begin{aligned}\chi_S(T) = &\left(\frac{d^2h}{dm_l^2}\right)v(T) + \left(\frac{dh}{dm_l}\right)^2\\ &\times\int_T dx\{\langle\mathcal{T}\tilde{\sigma}(x)\tilde{\sigma}(0)\rangle - \langle\tilde{\sigma}\rangle^2(T)\}.\end{aligned} \tag{8}$$

The subtraction of $\langle\tilde{\sigma}\rangle^2$ in χ_S above ensures that the self-energy can be written in terms of standard connected Feynman diagrams (including 1PR contributions) and is free of contact divergences proportional to $\delta^{(4)}(k = 0)$. Nevertheless, we will work in the dimensional regularization (DR) scheme, so that $\delta^{(D)}(0)$ terms formally vanish [28]. Thus, we can write

$$\chi_S(T) = \left(\frac{d^2h}{dm_l^2}\right)v(T) + \left(\frac{dh}{dm_l}\right)^2\Delta_\sigma(k = 0; T), \tag{9}$$

where

$$\Delta_\sigma(k; T) = \frac{1}{k^2 + M_{0\sigma}^2 + \Sigma(k_0, \vec{k}; T)} \tag{10}$$

is the Euclidean propagator of the $\tilde{\sigma}$ field and $\Sigma(k_0, \vec{k}; T)$ is the self-energy, which in the thermal field theory framework depends separately on the space and time components of the 4-momentum k [29].

The coefficients of $v(T)$ and $\Delta_\sigma(s = 0; T)$ in (9) can be written in terms of v, $M_{0\sigma}$, and $M_{0\pi}$, using (6), as

$$\begin{aligned}\frac{dh}{dm_l} &= 2B_0v\left(\frac{M_{0\sigma}^2}{M_{0\sigma}^2 - M_{0\pi}^2}\right),\\ \frac{d^2h}{dm_l^2} &= 4B_0^2v\frac{2M_{0\sigma}^2 - 3M_{0\pi}^2}{(M_{0\sigma}^2 - M_{0\pi}^2)^2}.\end{aligned} \tag{11}$$

The result (9) allows us to relate the scalar susceptibility with the propagator of the scalar field. Note that the first term of that equation is meant to be negligible near chiral restoration since it vanishes proportionally to the light quark condensate. Another argument that leads to the same conclusion is the following: around the transition region, χ_S tends to become degenerate with the pseudoscalar pion susceptibility χ_π [30–32], confirmed in lattice simulations [4]. On the other hand, a Ward identity allows us to write $\chi_\pi = -\langle\bar{q}q\rangle_l/m_l$ at any temperature [4,22,33–35]. Therefore, near the transition, replacing $v(T) = -(dh/dm_l)^{-1}\langle\bar{q}q\rangle_l(T) = -m_l(dh/dm_l)^{-1}\chi_\pi(T) \simeq -m_l(dh/dm_l)^{-1}\chi_S(T)$ in the first term on the rhs of (9), that term is $\mathcal{O}(M_{0\pi}^2/M_{0\sigma}^2)$ suppressed with respect to $\chi_S(T)$ on the lhs of (9).

Therefore, near the transition, the scalar susceptibility is proportional to the $s = 0$ Euclidean scalar propagator, and its temperature behavior in that region is therefore dominated by the inverse self-energy of the lightest state, which in this case is the σ of the LSM:

$$\begin{aligned}\chi_S(T) &\simeq 4B_0^2v^2\left(\frac{M_{0\sigma}^2}{M_{0\sigma}^2 - M_{0\pi}^2}\right)^2\Delta_\sigma(k = 0; T)\\ \Rightarrow \frac{\chi_S(T)}{\chi_S(0)} &\simeq \frac{M_{0\sigma}^2 + \Sigma(k = 0; T = 0)}{M_{0\sigma}^2 + \Sigma(k = 0; T)}.\end{aligned} \tag{12}$$

We will refer to the above result as the saturated LSM approach, in which the scalar susceptibility is approximately described as the inverse of the self-energy of the lightest scalar state. A similar approach will be carried out and studied extensively in Secs. II B and IV for the UChPT framework. In the latter approach, the self-energy contribution is taken as the real part of the pole position in the 2RS of the complex $s = k^2$ plane for the pion scattering amplitude (in the center-of-momentum frame $\vec{k} = \vec{0}$). We will then use the present LSM analysis to study the above saturation approach, in particular to compare it with a strictly perturbative result for χ_S (see details below) so that we can use it as a test bed for the UChPT description, more realistic concerning the $f_0(500)$ pole determination.

The first step would be then to provide a well-defined calculation of the σ self-energy in the LSM including finite-temperature corrections. For clarity, we will stick to the perturbative approach in λ. Although, as we are about to check, the real values of λ needed to achieve reasonable phenomenological results are quite large [23], the one-loop corrections to the self-energy lie around a 15% at $T = 0$ [23]. Besides, as mentioned above, our main goal within the LSM is not to provide a reliable phenomenological description but to provide a better understanding of the different approximations for χ_S performed in this work, at least parametrically in λ.

The one-loop diagrams contributing to the sigma self-energy are given in Fig. 1. It is important to remark that a consistent perturbative expansion requires that $M_{0\sigma}^2, M_{0\pi}^2$ remain of $\mathcal{O}(1)$ in the λ expansion so that $k^2 + M_\sigma^2$ remains the leading order of the inverse propagator. Hence, using (6), all the one-loop self-energy contributions remain of $\mathcal{O}(\lambda)$. Namely, the contributions of every diagram in Fig. 1 read [26]

$$\begin{aligned}
\Sigma_a(k_0,\vec{k};T) &= -3\lambda(M_{0\sigma}^2 - M_{0\pi}^2)J(M_{0\pi};k_0,\vec{k},T),\\
\Sigma_b(k_0,\vec{k};T) &= -9\lambda(M_{0\sigma}^2 - M_{0\pi}^2)J(M_{0\sigma};k_0,\vec{k},T),\\
\Sigma_c(T) &= 3\lambda G(M_{0\pi},T),\\
\Sigma_d(T) &= 3\lambda G(M_{0\sigma},T),\\
\Sigma_e(T) &= -9\lambda\frac{M_{0\sigma}^2 - M_{0\pi}^2}{M_{0\sigma}^2}G(M_{0\pi},T),\\
\Sigma_f(T) &= -9\lambda\frac{M_{0\sigma}^2 - M_{0\pi}^2}{M_{0\sigma}^2}G(M_{0\sigma},T),
\end{aligned} \tag{13}$$

where J and G are the finite-T integrals of the bubble and tadpole diagrams, respectively,

$$J(M_i;k_0,\vec{k},T) = T\sum_{n=-\infty}^{\infty}\int\frac{d^3\vec{p}}{(2\pi)^3}\frac{1}{p^2 - M_i^2}\frac{1}{(p-k)^2 - M_i^2}, \tag{14}$$

$$G(M_i,T) = T\sum_n\int\frac{d^3\vec{p}}{(2\pi)^3}\frac{1}{\omega_n^2 + \vec{p}^2 + M_i^2}, \tag{15}$$

and where $\omega_n = 2\pi nT$, $p = (i\omega_n,\vec{p})$, $k = (i\omega_m,\vec{q})$, and $i\omega_m \to k_0$ by analytic continuation, which can be performed after the Matsubara sums $\sum_n$ are carried out [29]. The divergent parts of the above loop integrals will be parametrized in DR. Their explicit expressions including finite parts can be found in Ref. [27] at $T = 0$. At $T \neq 0$, we write $G(M,T) = G(M,T=0) + g_1(M,T)$ with the g_1 function defined in Ref. [17]. As for the J function, we will only need $J(M;k_0,\vec{k} = \vec{0},T)$, the finite-temperature part of which can be found, for instance, in Refs. [19,36] and for $k_0 = 0$ satisfies $J(M;k=0,T) \equiv G_2(M,T) = -dG(M,T)/dM^2 = G_2(M,T=0) + g_2(M,T)$ with $g_2(M,T) = -dg_1(M,T)/dM^2$.

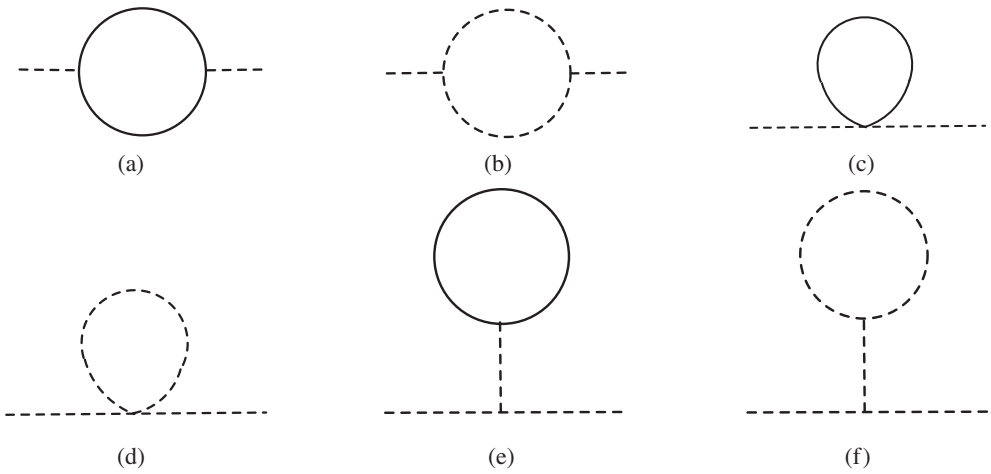

FIG. 1. One-loop contributions to the σ self-energy in the LSM. The solid lines represent the pion fields, and the dashed lines represent the sigma one.

As we are about to see, a standard LSM renormalization will allow us to express the self-energy as a finite quantity. Before that, we will provide a check of our result (9). From the Lagrangian (5), we have, within the perturbative λ expansion,

$$v(T) = \frac{d}{dh}\log Z = -\frac{1}{2}\frac{dM_{0\sigma}^2}{dh}G(M_{0\sigma},T) - \frac{3}{2}\frac{dM_{0\pi}^2}{dh}G(M_{0\pi},T) - \frac{1}{4\lambda}\frac{dM_{0\pi}^4}{dh} + \frac{dv^2}{dh}M_{0\pi}^2 + v^2\frac{dM_{0\pi}^2}{dh} + \mathcal{O}(\lambda^2)$$
$$= v\left[1 - \frac{3\lambda}{M_{0\sigma}^2}(G(M_{0\sigma},T) + G(M_{0\pi},T)) + \mathcal{O}(\lambda^2)\right] \tag{16}$$

$$\Rightarrow \langle\bar{q}q\rangle_l(T) = -2B_0v^2\frac{M_{0\sigma}^2}{M_{0\sigma}^2 - M_{0\pi}^2}\left[1 - \frac{3\lambda}{M_{0\sigma}^2}(G(M_{0\sigma},T) + G(M_{0\pi},T)) + \mathcal{O}(\lambda^2)\right]. \tag{17}$$

The above result is actually compatible with the mean-field approximation, where interactions and fluctuations are considered small (see Ref. [25] in the chiral limit). Taking one more mass derivative, we obtain then the purely perturbative expression for the scalar susceptibility:

$$\chi_S(T) = \frac{6B_0^2}{\lambda}[1 + \lambda(3G_2(M_{0\sigma},T) + G_2(M_{0\pi},T)) + \mathcal{O}(\lambda^2)]. \tag{18}$$

One can now check that we arrive exactly at the same result by expanding (9) in powers of λ and using our previous results (16) and (13).

Our next step will be to provide a finite and scale-independent result for the self-energy at finite temperature. The DR pole can be absorbed in the $T = 0$ renormalization of the pion and sigma masses,

$$M_{0\sigma}^2 - M_{0\pi}^2 = (M_\sigma^2 - M_\pi^2)\left[1 + \frac{6\lambda}{16\pi^2}\left(N_\epsilon + 1 - \log\frac{M_\sigma^2}{\mu^2} - \frac{1}{6}\right)\right] + O(\lambda^2), \tag{19}$$

$$M_{0\pi}^2 = M_\pi^2\left\{1 - \frac{3\lambda}{16\pi^2}\left[(N_\epsilon + 1)\left(1 - \frac{3M_\pi^2}{M_\sigma^2}\right) + \left(\frac{3M_\pi^2}{M_\sigma^2} - 2\right)\log\frac{M_\pi^2}{\mu^2} + \log\frac{M_\sigma^2}{\mu^2}\right]\right\} + O(\lambda^2), \tag{20}$$

with $N_\epsilon = 2/\epsilon - \gamma + \log 4\pi$ and μ the DR renormalization scale. The above renormalization coincides with that in the chiral limit provided by Ref. [27]. See also the $T = 0$ calculation of the σ propagator in Ref. [37]. With the above renormalization, we get the LSM one-loop self-energy finite and scale independent,

$$\Delta_\sigma^{-1} = M_\sigma^2 + \Sigma(k_0,\vec{k};T),$$
$$\Sigma(s,T=0) = \frac{3\lambda}{16\pi^2}(M_\sigma^2 - M_\pi^2)\left[\sigma_\pi(s)\log\left(\frac{\sigma_\pi(s)+1}{\sigma_\pi(s)-1}\right) + 3\sigma_\sigma(s)\log\left(\frac{\sigma_\sigma(s)+1}{\sigma_\sigma(s)-1}\right) + \log\left(\frac{M_\pi^2}{M_\sigma^2}\right) - \frac{13}{3}\right] + \mathcal{O}(\lambda^2),$$
$$\Sigma(k_0,\vec{k};T) = \Sigma(s,T=0) + 3\lambda\left\{\frac{3M_\pi^2 - 2M_\sigma^2}{M_\sigma^2}[g_1(M_\pi,T) + g_1(M_\sigma,T)]\right.$$
$$\left. - (M_\sigma^2 - M_\pi^2)[\delta J(M_\pi;k_0,\vec{k},T) + 3\delta J(M_\sigma;k_0,\vec{k},T)]\right\} + \mathcal{O}(\lambda^2), \tag{21}$$

where

$$\sigma_i(s) = \sqrt{1 - \frac{4M_i^2}{s}} \tag{22}$$

is the two-particle phase space and $\delta J(M;k,T) = J(M;k,T) - J(M;k,0)$.

The pole of the propagator and its evolution with temperature can now be readily calculated. Perturbatively, the pole of the propagator is at $s_p = M_\sigma^2 + \Sigma(k^2 = M_\sigma^2)$, which we will parametrize as is customary as $s_p = (M_p - i\Gamma_p/2)^2$. At $T \neq 0$, it will be enough for the purposes of this work to consider the pole at $\vec{k} = \vec{0}$. At $T = 0$, we get, for $M_\sigma > 2M_\pi$,

$$\mathrm{Re}s_p = M_\sigma^2 + \frac{3\lambda(M_\sigma^2 - M_\pi^2)}{16\pi^2}\left[-\frac{13}{3} + \sqrt{3}\pi + \log\left(\frac{M_\pi^2}{M_\sigma^2}\right) + \sigma_\pi(M_\sigma^2)\log\left|\frac{\sigma_\pi(M_\sigma^2)+1}{\sigma_\pi(M_\sigma^2)-1}\right|\right], \tag{23}$$

$$\mathrm{Im}s_p = -\frac{3\lambda(M_\sigma^2 - M_\pi^2)}{16\pi}\sigma_\pi(M_\sigma^2), \tag{24}$$

which agrees with the result in Ref. [38] in the chiral limit. Following Ref. [23], we will set our reference values for the numerical parameters of the model as those for which the σ pole values lie near the experimental determination for the $f_0(500)$ in the PDG [16], namely, $M_p^{\mathrm{PDG}} \simeq (400-550)\,\mathrm{MeV}$, $\Gamma_p^{\mathrm{PDG}} \simeq (400-700)$ MeV. As noted in Ref. [23], there is no way to accommodate the LSM parameters to get good agreement both for M_p and Γ_p. We show in Fig. 2 the dependence on λ of M_p and Γ_p for the physical $M_\pi = 140$ MeV, which confirms the previous statement. In our numerical results, we have taken for the tree-level $M_\sigma^2 = M_\pi^2 + 2\lambda F_\pi^2$ with $F_\pi \simeq 93$ MeV. In view of those results, we select as a reference range for our numerical results the interval $\lambda \sim 10$–20 where the deviations from the PDG value are not large in either M_p or Γ_p, the lower (higher) value of λ favoring M_p (Γ_p) as shown for some sample values in Table I, in which we also include the chiral limit values. In turn, we note that, even though the typical λ values needed are large, the one-loop corrections remain reasonably under control, lying between 10%–15% for the corrections to M_p compared to the tree-level M_σ.

Our next step will be to provide the results for the different approaches to the scalar susceptibility mentioned above. Taking the $k \to 0^+$ limit for the self-energy, we can get $\chi_S(T)$ from the saturated approach (12). From (21), taking into account that

$$\lim_{s\to 0}\sigma_i(s)\log\frac{\sigma_i(s)-1}{\sigma_i(s)+1} = -2,$$

we have

$$\Sigma(k=0;T) = \frac{\lambda}{16\pi^2}(M_\sigma^2 - M_\pi^2)\left[11 + 3\log\left(\frac{M_\pi^2}{M_\sigma^2}\right)\right] + 3\lambda\left\{\frac{3M_\pi^2 - 2M_\sigma^2}{M_\sigma^2}[g_1(M_\pi,T) + g_1(M_\sigma,T)] - (M_\sigma^2 - M_\pi^2)[g_2(M_\pi,T) + 3g_2(M_\sigma,T)]\right\} + \mathcal{O}(\lambda^2). \tag{25}$$

In Fig. 3, we show our results for $\chi_S(T)$ in the saturated approach, compared to the perturbative one arising from (18). For an easier comparison with lattice data and with our results in Secs. II B and III, we are using for the saturated LSM susceptibility the following normalization:

$$\chi_S^{\mathrm{sat,LSM}}(T) = A\frac{M_\pi^4}{4m_l^2}\frac{M_{0\sigma}^2 + \Sigma(k=0;T=0)}{M_{0\sigma}^2 + \Sigma(k=0;T)}. \tag{26}$$

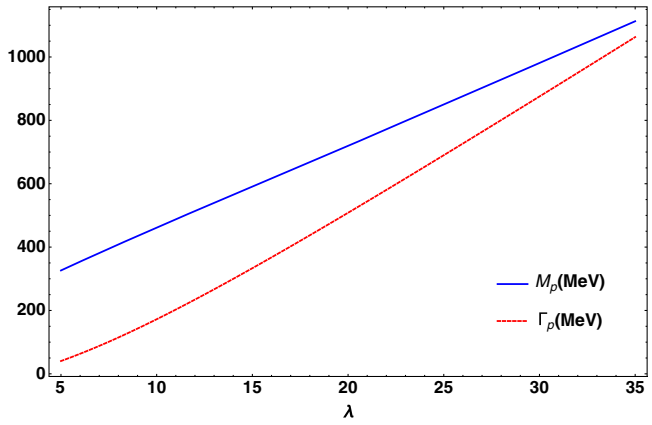

FIG. 2. Pole parameters M_p and Γ_p in the one-loop LSM as a function of λ for the physical mass M_π.

For the results in Fig. 3, we have taken $A = A_{\mathrm{ChPT}} \simeq 0.15$ as in Sec. II B (see comments below). Nevertheless, the corresponding value for the normalization constant A from the normalization given in (12) would be around $A_{\mathrm{LSM}} \approx 4F_\pi^2/M_S^2(0) \approx 0.07$–$0.17$ for the range of values shown in Table I and hence compatible with the ChPT value.

The main conclusion that we extract from the results shown in Fig. 3 is that the saturated approach provides a

TABLE I. Pole mass and width at $T = 0$ for sample values of λ, with $M_p = \mathrm{Re}\sqrt{s_p}$ and $\Gamma_p = -2\mathrm{Im}\sqrt{s_p}$.

M_π (MeV)	M_p (MeV)	Γ_p (MeV)	λ
0	450.0	172.5	8.4
0	775.1	550.0	20.0
140	450.0	159.2	9.6
140	750.1	550.0	21.2

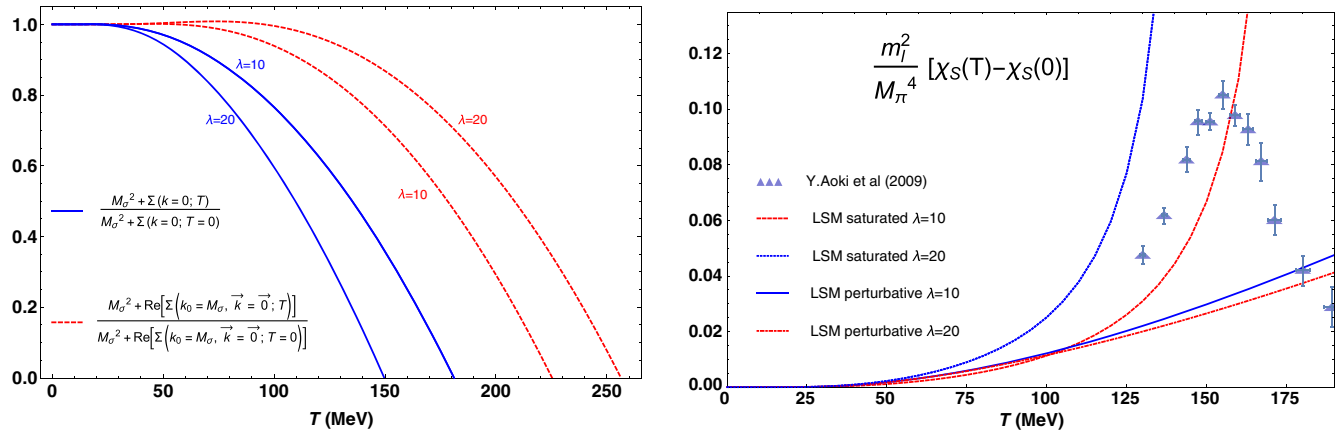

FIG. 3. Left: LSM thermal self-energy at $k = 0$ and at $k_0 = M_\sigma$, $\vec{k} = \vec{0}$, for the range $\lambda = 10$–20. Right: Saturated susceptibility in the LSM compared to lattice data and to the purely perturbative one. In both figures, $M_\pi = 140$ MeV. The lattice data and errors are from Ref. [1].

much stronger growth with temperature than the purely perturbative one, actually covering lattice data below the transition for the range of values of $\lambda \sim 10$–20 corresponding to the $T = 0$ poles in Table I. However, the saturated susceptibility actually diverges around the transition point, even in the massive case, and therefore is not able to reproduce either the crossover peak. As we will see in Sec. II B, the UChPT approach will considerably improve this behavior. Nevertheless, an important comment is that, even within this LSM approach, which has its own limitations, as we are discussing here, a saturated description of the scalar susceptibility in terms of the thermal self-energy seems to be able to describe lattice data reasonably without adding additional degrees of freedom. That feature is shared also by the UChPT approach and is one of the main conclusions of this work. Finally, in Fig. 3, we have shown also a comparison of the $s = 0$ result for the self-energy temperature dependence with the same approach evaluating the real part of the self-energy at $s = s_p$, the latter being the point at which the equivalent of the self-energy is naturally evaluated within the UChPT approach (see details in Sec. II B). The qualitative behavior is the same, although numerically the temperature at which the self-energy vanishes (divergent susceptibility) moves to a higher value. In both cases, the dropping behavior can be understood as a chiral symmetry restoration tendency, since $M_\sigma^2 + \mathrm{Re}\Sigma$ corresponds to the T-dependent scalar mass, which means it drops below the transition approaching the pion mass [25].

B. Unitarized chiral perturbation theory: Thermal $f_0(500)$ saturation approach

The LSM description discussed in the previous section relies on the one-loop λ expansion. However, as we have just seen, the typical numerical λ values needed to reproduce meson observables are large, in particular to reconcile both the real and imaginary parts of the $f_0(500)$ pole at $T = 0$ found in the one-loop LSM with the experimentally observed range for those quantities. In addition, the σ stable state in the Lagrangian formulation is not well justified physically.

A well-established framework to generate the $f_0(500)$, without having to appeal to an explicit σ-field Lagrangian realization, is UChPT. One starts from the ChPT series for the $\pi\pi$ scattering amplitude in a given channel, projected into partial waves of well-defined isospin I and angular momentum J [27], namely, $t^{IJ}(s,T) \simeq t_2^{IJ}(s) + t_4^{IJ}(s,T) + \cdots$. The t_4 contribution contains one-loop diagrams from the second-order ChPT Lagrangian as well as tree-level terms from the fourth-order one proportional to LECs. The temperature corrections arise in loops and are therefore included from the t_4 contribution onward [19]. The ChPT series ensures the model-independent low-energy behavior and is unitary only perturbatively, i.e., $\mathrm{Im}t_4 = \sigma_\pi |t_2|^2$ for $s \geq 4M_\pi^2$ and so on, with σ_π the two-pion phase space defined in (22).

An exactly unitary amplitude can be constructed by several methods. The main method we will follow here is the $\mathcal{O}(p^4)$ inverse amplitude method (IAM), originally developed at $T = 0$ in Ref. [39] and extended to finite temperature in Ref. [20]. In that approach, exact unitarity and matching to the low-energy ChPT expansion are demanded, including the finite-temperature corrections to the scattering amplitude in the center-of-momentum frame, which implies the modification of the phase space

$$\sigma_T(s,T) = \sigma_\pi[1 + 2n_B(\sqrt{s}/2, T)], \tag{27}$$

with $n_B(x,t) = [\exp(x/T) - 1]^{-1}$ the Bose-Einstein distribution function, so that perturbatively $\mathrm{Im}t_4(s,T) = \sigma_T(s,T)|t_2(s)|^2$ for $s \geq 4M_\pi^2$.

Thus, the unitarized IAM partial waves read

$$t_{\mathrm{IAM}}(s;T)=\frac{t_2(s)^2}{t_2(s)-t_4(s,T)}. \tag{28}$$

The above amplitude is analytic off the real axis and satisfies the exact thermal unitarity relation $\mathrm{Im}t_{\mathrm{IAM}}=\sigma_T|t_{\mathrm{IAM}}|^2$ for $s\geq 4M_\pi^2$. As a consistency check, this relation has been shown to hold exactly within the large-N_{GB} approach in the chiral limit, in which N_{GB} is the number of Goldstone bosons [40]. In addition, the IAM amplitude reproduces the ChPT series up to $\mathcal{O}(p^4)$ when expanded at low energies and is analytical in the complex s plane [20], which ultimately allows us to search for resonances as poles in the 2RS. Thus, the $f_0(500)$ ($I=J=0$) and the $\rho(770)$ ($I=J=1$) are generated at $T=0$ with their pole position parameters $s_p=(M_p-i\Gamma_p/2)^2$ in agreement with those quoted experimentally by the PDG [16]. For the $f_0(500)$, taking the LEC given in Ref. [41], which we will use throughout this work, one gets $M_p=442.66$ MeV and $\Gamma_p=433.0$ MeV at $T=0$.

According to our discussion in Sec. II A, we expect the scalar susceptibility $\chi_S(T)$ to be proportional to the inverse of $\Sigma(k=0)$, Σ denoting generically the self-energy of the $f_0(500)$ state. However, within the UChPT approach, the $f_0(500)$ state is dynamically generated and then emerges as a 2RS pole of the scattering amplitude rather than a time-ordered product or thermal correlator, as in the case of the LSM discussed in the previous section. Thus, within UChPT, instead of Σ, we have access to the pole parameters of the $f_0(500)$ state, namely, M_p, Γ_p, and $g_{\sigma\pi\pi}$, the effective $\sigma\pi\pi$ effective coupling [23], so that the 2RS amplitude reads around the pole

$$t^{II}=\frac{1}{16\pi}\frac{g_{\sigma\pi\pi}^2}{s-s_p}+\cdots, \tag{29}$$

and the dots denote subdominant terms around $s\sim s_p$. Note that if we regard (29) as the exchange of a scalar state f_0 the self-energy of such a state would satisfy $\Sigma_{f_0}(s_p)=s_p$, where we have included in Σ_{f_0} the equivalent of the tree-level mass. On the other hand, $\mathrm{Im}\Sigma_{f_0}(k=0)=0$ since at $k=0$ there are no decay channels open so that, assuming that the sensitivity of $\mathrm{Re}\Sigma_{f_0}$ from s_p to $s=0$ lies within the typical uncertainty range of this approach, which we will analyze in detail below, we are led to the definition of the unitarized scalar susceptibility, which corresponds to the saturated thermal $f_0(500)$ state approach within UChPT,

$$\chi_S^U(T)=A\frac{M_\pi^4}{4m_l^2}\frac{M_S^2(0)}{M_S^2(T)}, \tag{30}$$

where we follow the same normalization as in Sec. II A and where the scalar thermal pole mass (defined as the real part of self-energy at the pole) is

$$M_S^2(T)=\mathrm{Re}s_p(T)=M_p^2(T)-\frac{1}{4}\Gamma_p^2(T), \tag{31}$$

the temperature dependence of $M_p(T)$ and $\Gamma_p(T)$ being determined from the 2RS pole of the unitarized amplitude (28), as discussed above. The thermal mass definition (31) shows a dropping behavior compatible with the expected chiral restoring features discussed in Sec. II A, unlike the $I=J=1$ channel, in which the mass has a much softer T dependence [20,22]. Moreover, in Ref. [22], it has been shown that if the normalization A is chosen to match the perturbative ChPT one-loop result for χ_S at $T=0$, i.e.,

$$A_{\mathrm{ChPT}}=\frac{4m_l^2}{M_\pi^4}\chi_S^{\mathrm{ChPT}}(0)=\frac{\chi_S^{\mathrm{ChPT}}(0)}{B_0^2}\simeq 0.15, \tag{32}$$

the resulting χ_S^U follows closely the ChPT curve for low temperatures and develops a maximum at a temperature around 157 MeV (with the LECs used in Ref. [22]), supporting strongly our previous assumptions. One of our main purposes here is to test in a more quantitative way the reliability of that saturated approach to describe lattice data, as compared with other approaches such as the HRG discussed in Sec. III, the LSM described in Sec. II A, or $\chi_S(T)$ obtained perturbatively in ChPT or the virial approach [18].

The theoretical uncertainties involved in χ_S^U in (30) can be parametrized into three main types: the normalization factor A, the choice of the unitarization method, and the numerical uncertainties of the LEC involved in $\pi\pi$ scattering for the pole determination. Here, we will analyze in detail the sensibility of this approach to those three sources, focusing on its description of lattice data at finite temperature while complying with the $T=0$ predictions for scattering data, the $f_0(500)$ pole, and the ChPT low-energy approach.

Let us consider first the LEC dependence. As stated above, we will use as a reference set of LECs those given in [41], namely,

$$\begin{aligned} l_1^r&=-(3.7\pm 0.2)\times 10^{-3}, & l_2^r&=(5.0\pm 0.4)\times 10^{-3},\\ l_3^r&=(0.8\pm 3.8)\times 10^{-3}, & l_4^r&=(6.2\pm 5.7)\times 10^{-3}, \end{aligned} \tag{33}$$

where l_i^r are the SU(2) renormalized LECs according to the notation in Ref. [27], evaluated at a DR scale $\mu=770$ MeV. The above LECs were obtained by a fit of the IAM to scattering data, leaving l_3^r and l_4^r fixed to their original ChPT values in Ref. [27]. We remark that the LECs appearing in the $\pi\pi$ scattering vertices are $l_{1,2}^r$ and are those to which the pole position parameters of resonances are most sensitive, while $l_{3,4}^r$ arise from the renormalization of the pion mass M_π and the pion decay constant F_π.

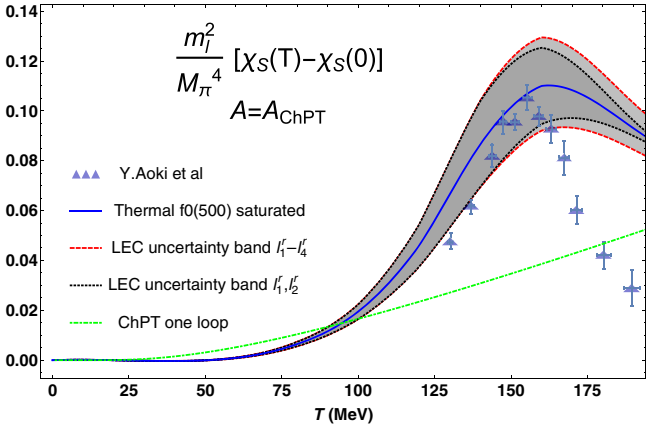

FIG. 4. Results for the $f_0(500)$ saturated scalar susceptibility (30) normalized with A_{ChPT} in (32) including the uncertainties coming from the LECs (33). The lattice data and errors are from Ref. [1]. The central curves corresponding to the two uncertainty bands shown lie on top of each other.

We will estimate the range of variation of the saturated susceptibility by considering, for every T, the mean square error of the results obtained for the eight combinations of upper and lower values given by (33). The resulting uncertainty band is shown in Fig. 4, in which the central line corresponds to the average value and in which we compare our prediction for χ_S based on the saturated thermal $f_0(500)$ approach, with lattice data coming from the work [1], the results of which can be easily translated into our present normalization. We consider also in the figure the uncertainty band generated solely by l_1^r and l_2^r, which as we see remains very close to the band of the four LECs, confirming our previous observation about the sensitivity of the pole parameters to the LECs. We also include in the figure the one-loop ChPT curve with the LECs given in Ref. [18]. Note that the ChPT result lies close to the LSM perturbative one in Fig. 3 since the leading behavior in the LSM result (18) comes from $g_2(M_\pi, T)$, which is precisely the ChPT pion gas contribution [18].

These results lead to interesting conclusions: as we had anticipated, the saturated UChPT result reproduces the expected crossover peak around the transition and hence improves over the saturated LSM in Sec. II A. We will actually see here that the adequate description of the $T = 0$ pole of the UChPT result, as well as other basic requirements such as analiticity and unitarity, produce this behavior. Moreover, most of the lattice data fall into the uncertainty band, the approach being especially adequate near the transition region. Put in different words, one could use the LECs as fit parameters to reproduce the lattice χ_S at finite temperature, and the results of the fit would be in the range allowed by the $T = 0$ determinations of those LECs based on experimental information.

Nevertheless, it would be reassuring to consider other ways to test the robustness of the unitarized approach. For that reason, let us consider another possible theoretical source of uncertainty, the unitarization method, which in turn will allow us to understand better which are the essential requirements that we should incorporate in the unitarized approach.

As mentioned above, the IAM satisfies unitarity for partial waves and reproduces the two first terms of the ChPT series at low energies, i.e., $t_2 + t_4$. If we relax the second condition only to t_2, this leads to the so called K-matrix amplitude (see, for instance, the discussion in Refs. [23,42]),

$$t_K(s;T) = \frac{t_2(s)}{1 - \sigma_T(s,T)t_2(s)}, \tag{34}$$

where we have used that $\mathrm{Im}t_4(s,T) = \sigma_T t_2(s)^2$ for $s \geq 4M_\pi^2$. Although the above amplitude is unitary, it is not analytic due to the phase space factor $\sigma_T(s,T)$, so it cannot be properly extended to the complex s plane, in particular to define properly the 2RS. The requirement of analyticity is then crucial, as satisfied, for instance, by the IAM. With some modifications with respect to (34), we can construct a unitary, analytical amplitude, different from the IAM and based on the so-called chiral unitary approach [43] as

$$t_{U\mathrm{mod}}(s;T) = \frac{t_2^2(s)}{t_2(s) - t_{4J}(s,T)}, \tag{35}$$

with

$$t_{4J}(s,T) = t_4(s,0) + 16\pi t_2(s)^2[J(M_\pi; k_0 = \sqrt{s}, \vec{k} = \vec{0}, T) - J(M_\pi; k_0 = \sqrt{s}, \vec{k} = \vec{0}, T = 0)] \tag{36}$$

and J the loop thermal integral defined in (14), which comes from the s-channel $\pi\pi$ scattering amplitude in the center-of-momentum frame, responsible for the unitarity contribution [19].

The unitarized amplitude (35) can be understood as obtained from (34) by replacing the $\sigma_T(s,T)$ contribution in the denominator by an analytic function in s satisfying unitarity, since $\mathrm{Im}J(s,T) = \sigma_T(s,T)/(16\pi)$ for $s \geq 4M_\pi^2$.

Note that we keep the full t_4 ChPT amplitude at $T = 0$. The reason is that we are renormalizing the $T = 0$ divergent part of the integral (14), dimensionally regularized, following the standard ChPT prescription [27], i.e., absorbing the divergence in the LECs. On the other hand, since we are using the LECs in Ref. [41], fitted with the full IAM, to be consistent, we have to ensure that the modified amplitude (35) reduces at $T = 0$ to the IAM one in (28).

This guarantees also that the $T = 0$ $f_0(500)$ pole remains at the same value, compatible with the PDG, with these two different unitarization methods at finite temperature. In addition, in this way, we will be able to test again the sensitivity to the LEC uncertainties in (33). As for the finite-temperature correction in (35), we are taking the minimal contribution ensuring unitarity and analyticity, i.e., the T-dependent part of $J(s, T)$. As we are about to see, keeping the three requirements of analiticity, unitarity, and the $T = 0$ pole leads to a qualitative behavior compatible with the crossover.

In Fig. 5, we plot the resulting $M_S^2(T)$ defined in (31), with the two methods we have discussed, i.e., the IAM and the $U_{\rm mod}$ ones. We also consider the same function taking the light chiral limit ($M_\pi \to 0^+$) in our expressions [recall that the l_i^r in (33) are mass independent]. We observe that the qualitative behavior around the transition is the same with both methods; i.e., they both develop a minimum around $T \simeq 150$ MeV in the massive case. However, we see that the curve of the $U_{\rm mod}$ method reaches zero before the minimum, which would give rise to a divergent susceptibility at that point, pretty much like the LSM saturated approach in Sec. II A except that in the LSM the thermal mass does not develop a minimum. That difference between the two methods remains when the uncertainty bands for the LEC are included. In that figure, we also show the constant M_π^2 reference value. The fact that the two methods give rise to a decreasing function approaching the pion mass squared strengthens the interpretation of $M_S^2(T)$ as a scalar mass, since $O(4)$ restoration would imply the degeneration of $\sigma - \pi$ states, while the thermal dependence of the pion mass is meant to be smooth [44].

Therefore, the requirements of thermal unitarity and analyticity, together with the $T = 0$ pole prediction, guarantee the key qualitative features of a crossover behavior in terms of the position of the minimum as compared to the lattice prediction for T_c, reasonably maintained within the LEC uncertainty band. This is then a robust result. However, the additional requirement, only fulfilled by the IAM, of complying with the ChPT thermal scattering amplitude up to fourth order is needed to describe the scalar susceptibility accurately.

The previous difference between the two methods is washed out in the chiral limit, as Fig. 5 shows. There, both methods yield results compatible among them within the LEC uncertainty band, predicting a critical temperature at which the scalar mass vanishes, which is consistent with the expected reduction of the lattice T_c of around 15%–20% in the chiral limit [3].

Our results in this section might seem somehow striking, since we are describing a thermodynamical observable near the transition with just one effective state, the thermal $f_0(500)$, without using the information coming from the rest of the hadronic spectrum. Qualitatively, we had observed the same feature in the LSM in Sec. II A. Actually, this is our main motivation to compare the UChPT analysis with the HRG approximation described in Sec. III. In this regard, one must take into account that, as stated above, $\chi_S(T)$ is precisely the observable where the lightest scalar state is meant to dominate, while this conclusion may not be extensible to other quantities such as the quark condensate. Thus, the thermal unitarization procedure seems to incorporate in a natural way the relevant information of higher-order states, encoded precisely in the LECs. Our results may at first seem at odds with the usual claim within the HRG approach stating that the $f_0(500)$ state can be ignored in the list of hadron states contributing to the partition function, motivated partly by a cancellation between the $IJ = 00$ and $IJ = 20$ channels in the $T = 0$ partial waves when considering the virial expansion [18,45] in which those channels appear weighted by the $(2I + 1)(2J + 1)$ factor. However, it is important to

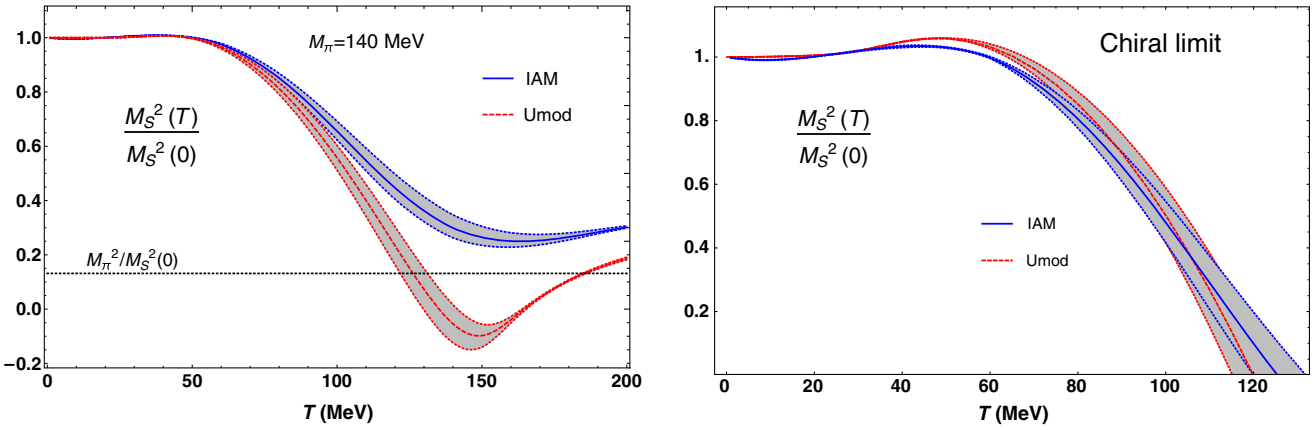

FIG. 5. Squared scalar $f_0(500)$ thermal mass as defined by (31), calculated with the IAM and Umod unitarization methods in (28) and (35), respectively. Left: for the physical pion mass, where we show the pion mass squared value. Right: in the chiral limit. In both cases, the bands reflect the uncertainties in the LECs l_1^r and l_2^r given in (33) with l_3^r and l_4^r fixed at their central values.

point out that we are including here, as a key ingredient, the *thermal* corrections to the $\pi\pi$ scattering amplitude, which include higher-order finite-T corrections not included in the usual virial approach, in which scattering is included only at $T = 0$. Those thermal corrections, as explained above, account for the thermal unitarity processes giving rise ultimately to the main modifications of the $f_0(500)$ pole parameters, directly connected with chiral symmetry restoration as we are seeing here.

In connection with the last comment, one may wonder what would be the effect of the $f_0(500)$ state and its thermal modifications in other observables relevant in heavy ion collisions, such as hadron multiplicities and yields. The latter have been successfully described within the so-called thermal statistical models, very much in the same spirit as the HRG [46–49] (see Sec. III) in which the different PDG states contribute through their free partition function, and the resonances width can be incorporated by integrating in energy with a suitable Breit-Wigner shape [46]. The decay channels of those resonances feed the hadron yields at chemical freeze-out. Following this approach, the effect of including the $f_0(500)$ was first studied in Ref. [47], resulting in a few percent increase in the pion yield from the $\pi\pi$ decay channel. That analysis showed also little dependence on variations of the $f_0(500)$ mass and width, which would lead to the conclusion that the finite-T corrections we are discussing here would not have a significant effect for those observables. Regarding the connection with the QCD phase transition, hadron yields and multiplicities are correlated to hadronization rather than to chiral symmetry [49], and hence we would expect a smaller effect of the $f_0(500)$ modifications addressed in the present work.

However, as we have discussed above, the $f_0(500)$ should be treated as a broad resonance, and hence the Breit-Wigner approach is not quite adequate in that case. In addition, as we have just mentioned, the $IJ = 20$ repulsive channel would produce a cancellation of the $f_0(500)$ effect that has to be accounted for. Such an analysis has been performed in Ref. [45] within the virial approach, showing that such a cancellation takes place also for the pion yield, resulting in a much smaller effect, around a 0.3% decrease. Within that approach, the quantity controlling the particle spectra for those channels and hence the pion yield and multiplicity is

$$d_{IJ}(E) = \frac{1}{\pi}\frac{d\delta_{IJ}(E)}{dE}, \tag{37}$$

with $E = \sqrt{s}$ and δ_{IJ} the corresponding IJ channel phase shift. Thus, to provide here a rough estimate of the possible effects of the $f_0(500)$ spectral modifications, we have calculated the $d_{00}(E)$ and $d_{20}(E)$ distributions in (37) with the phase shifts obtained from the IAM, both at $T = 0$ and at $T = 156$ MeV, which is the freeze-out temperature considered in Ref. [45]. The result is that the qualitative picture that we have just described with $T = 0$ phase shifts does not change much for the isospin-weighted combination $(2I + 1)(2J + 1)d_{IJ}$, the modification being smaller as E increases. The modifications for the individual d_{IJ} follow a similar behavior.

The previous arguments indicate that the thermal effects on the $f_0(500)$ discussed here are not expected to produce large corrections regarding the pion multiplicity and yield, unlike the case of the scalar susceptibility. A different story, though, would be the study of correlations such as $\pi^+\pi^-$, which are not isospin averaged so that the previous cancellation does not occur [45]. In this sense, a promising line of research is the analysis of correlations and fluctuations in heavy ion collisions and their connection with the QCD phase diagram [50].

Generally speaking, it would be interesting to examine how the thermal dependence of other PDG states can affect different observables, including hadron yields and correlations. Although such an analysis is beyond the scope of this work, there are significant examples of light mesons which might be of interest. Apart from the ρ meson and its well-known influence in the photon and dilepton spectrum, already mentioned in the Introduction, other relevant states which are in the line of our present approach are the κ and a_0 mesons, which play a crucial role in understanding the pattern of chiral symmetry restoration in connection with the $U(1)_A$ symmetry [51].

III. HADRON RESONANCE GAS APPROACH

The results in the previous sections show that one can actually describe correctly the lattice results for the scalar susceptibility, saturating it with just the contribution from the thermal $f_0(500)$ state. On the other hand, one would expect that any thermodynamical quantity should be sensitive to higher-order hadron states as the transition point is approached, according to the standard framework of the HRG, as we have mentioned before. Therefore, the inclusion of the thermal effects in the $f_0(500)$ pole and the LEC dependence somehow account effectively for the effect of those states, generating novel additional features such as the crossoverlike behavior discussed in the previous section. To make this comparison more clear, we will provide in this section the result for the scalar susceptibility within the HRG approach, which, as stated in the Introduction, has been used extensively in the literature to describe the hadron gas below the transition.

The free energy density in the simplest HRG approximation, i.e., considering only free resonant states without including their width or their interactions, is given by [9–13,15]

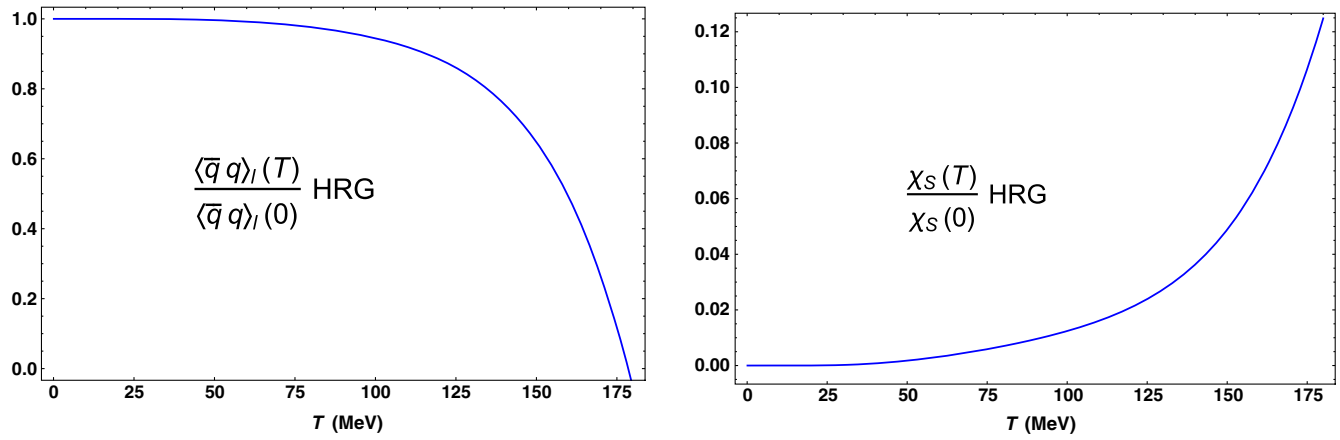

FIG. 6. Light quark condensate and scalar susceptibility in the hadron resonance gas approach described in the main text.

$$z(T) = z_M(T) + z_B(T),$$
$$z_{M,B}(T) = \pm T \sum_{M,B} d_i \int \frac{d^3\vec{p}}{(2\pi)^3} \log\left[1 \mp e^{-\beta E_i(p)}\right], \quad (38)$$

where $E_i = \sqrt{|\vec{k}|^2 + M_i^2}$, M and B stand for the meson and baryon contributions, the upper sign is for mesons, and the lower one is for baryons. The sum extends to hadron states with degeneracy d_i and mass M_i quoted in the PDG [16]. In this work, we will consider only hadron states up to $M = 2$ GeV, following Ref. [15].

From the pressure or the free energy density, one can, in principle, derive straightforwardly the quark condensate and the scalar susceptibility according to (1) and (2). However, the HRG formulation is parametrized in terms of hadron masses, so any calculation involving quark mass derivatives requires modeling the hadron mass dependence on quark masses. Several approximations for such a dependence have been followed in the literature within the HRG context, starting from a simple linear dependence of the form $\frac{\partial M_h}{\partial M_\pi^2} = 2C$ with constant C [9,11] to more elaborate ones [10,12,13,15]. Here, we will follow the approach in Refs. [12,15], which gives a good fit for the quark condensate to the $N_t = 12$ lattice data in Ref. [1], used here as a lattice reference set of data for both the quark condensate and for the scalar susceptibility. Within that approach, the dependence of pseudo Nambu-Goldstone bosons, i.e., pion, kaon, and eta masses, is extracted directly from the one-loop ChPT calculation [52], while the masses of the rest of the hadrons are taken to scale within a constituent quark picture as

$$\frac{\partial M_B}{\partial m_{l,s}} = (3 - N_s)\frac{\partial M_l}{\partial m_{l,s}} + N_s \frac{\partial M_s}{\partial m_{l,s}},$$
$$\frac{\partial M_M}{\partial m_{l,s}} = (2 - N_s)\frac{\partial M_l}{\partial m_{l,s}} + N_s \frac{\partial M_s}{\partial m_{l,s}}, \quad (39)$$

where the constituent masses M_l and M_s for light and strange quarks are extracted from the Nambu-Jona-Lasinio model calculation in Ref. [53]. We follow Ref. [15] for the assignments of the hadron strangeness content for open and hidden strange mesons, as well as for singlet and octet members.

We show in Fig. 6 the light quark condensate and the scalar susceptibility within the HRG approach. As it is known, within this approach, the quark condensate drops monotonically and vanishes at a given temperature, for physical quark masses. There is a substantial reduction with respect to ChPT in the transition temperature, estimated here as the vanishing condensate point, when all the hadron degrees of freedom are included. The value obtained from the plot in Fig. 6 is $T_c \simeq 178.5$ MeV, while the value obtained, for instance, in ChPT with three-loop pion interactions [17], or in the virial approach [18], is around $T_c \simeq 250$ MeV. We will actually see in the next section that allowing some uncertainty in the normalization of the HRG expressions, to account in a simple way for the different uncertainties involved, allows for a fairly good description of lattice data.

As for the scalar susceptibility, the HRG approach shown here (and not calculated before to the best of our knowledge) gives rise to a monotonically increased function, just as ChPT or virial approaches [17,18], i.e., not reproducing the transition crossover peak. Also in the next section, we will carefully explore to what extent the HRG approach can describe simultaneously the quark condensate and susceptibility lattice results.

IV. FITS TO LATTICE DATA

In this section, we will perform a more detailed analysis of the description of lattice data within the theoretical framework developed in this work. We will concentrate mostly in the scalar susceptibility, since, as explained before, this is the thermodynamic observable for which

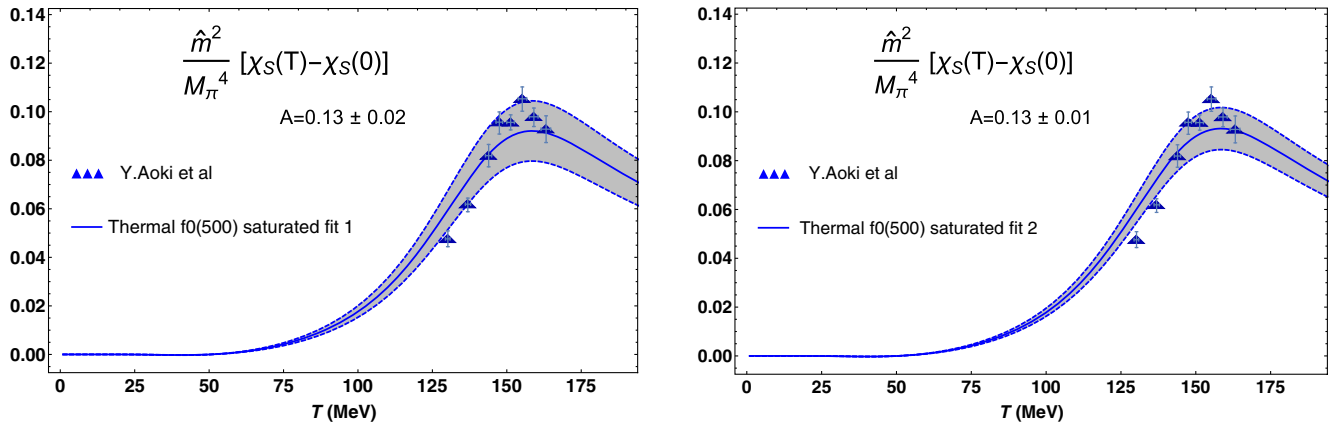

FIG. 7. Fits of the thermal $f_0(500)$ saturated scalar susceptibility with the normalization constant as a fit parameter and with the central values of the LEC given in (33). Fit 1 corresponds to fitting data up to $T \leq T_c = 155$ MeV, while in fit 2, we include two more lattice points, up to $T = 163$ MeV. The quoted uncertainties in the A parameter and the bands correspond to the 95% confidence level of the fit. The lattice data and errors are from Ref. [1].

the role of the thermal $f_0(500)$ is expected to be more important. In particular, we will compare the description provided by the thermal $f_0(500)$ saturation approach with that of the HRG, in a more quantitative way.

For an effective way to parametrize the uncertainties in both approaches, we will allow for a normalization constant, which we will consider as our fit parameter. Thus, in the thermal $f_0(500)$ saturation definition (30), we fit the A parameter instead of fixing it to its ChPT value, which accounts at least partially for the uncertainties inherent of this method and discussed in Sec. II B. The results we have obtained in Sec. II B show that we could alternatively fit the LECs within their $T = 0$ uncertainties to get a good description of lattice points, especially around the transition peak. As for the HRG approach, we normalize $z \to Bz$ in (38) as a simple way to parametrize the uncertainties in this approach such as the quark mass dependence of hadron masses, the upper limit of the resonances included, or the absence of interactions and decay channels.

We show in Fig. 7 the results of two different fits of the thermal $f_0(500)$ saturated approach. The difference between those two fits is just the number of points included. Thus, in fit 2, we include two more points around the transition point. The result for the A parameter is shown in the figure, together with the uncertainty band corresponding to the 95% confidence level of the fit. The different fit parameters as well as the goodness of fit indicators are collected in Table II for all the fits performed in this section. Note that the values of A quoted in the table are compatible with the ChPT value in (32), and therefore the predictions of the fitted curve for lattice data do not spoil the expected $T = 0$ value for the scalar susceptibility, as given by the ChPT result.

On the other hand, in Fig. 8, we show the results of two fits with the HRG approach (HRG fits 1 and 2), corresponding to fit only the susceptibility lattice points, with the same sets of data used for fits 1 and 2 with the thermal $f_0(500)$ approach. We see that, as long as we keep the data points below T_c, the HRG gives a slightly better fit than the thermal $f_0(500)$ one, as would be naturally expected from a HRG approach. However, including only two more points around T_c worsens the HRG in favor of the $f_0(500)$ one, which is consistent with the different qualitative behavior of both curves around the maximum and confirms our previous comments about the role of the thermal $f_0(500)$.

Regarding the HRG description, an important observation must be taken into account: the values of B needed to fit the susceptibility are in conflict with those needed to fit the quark condensate. Let us justify this conclusion in detail. For that purpose, we consider the HRG result for the reduced quark condensate

$$\Delta_{l,s} = \frac{\langle \bar{q}q \rangle_l(T) - \frac{m_l}{m_s}\langle \bar{s}s \rangle(T)}{\langle \bar{q}q \rangle_l(0) - \frac{m_l}{m_s}\langle \bar{s}s \rangle(0)}, \tag{40}$$

TABLE II. Parameters for the different fits as explained in the main text.

Fit	A	B	χ^2/dof	R^2	$T_{\max}$ (MeV)
Thermal $f_0(500)$ fit 1	0.13 ± 0.02		6.25	0.986	155
Thermal $f_0(500)$ fit 2	0.13 ± 0.01		4.93	0.989	165
HRG fit 1		1.90 ± 0.02	1.33	0.997	155
HRG fit 2		1.71 ± 0.23	10.30	0.978	165
HRG fit 3		1.06 ± 0.12	3.77	0.998	155

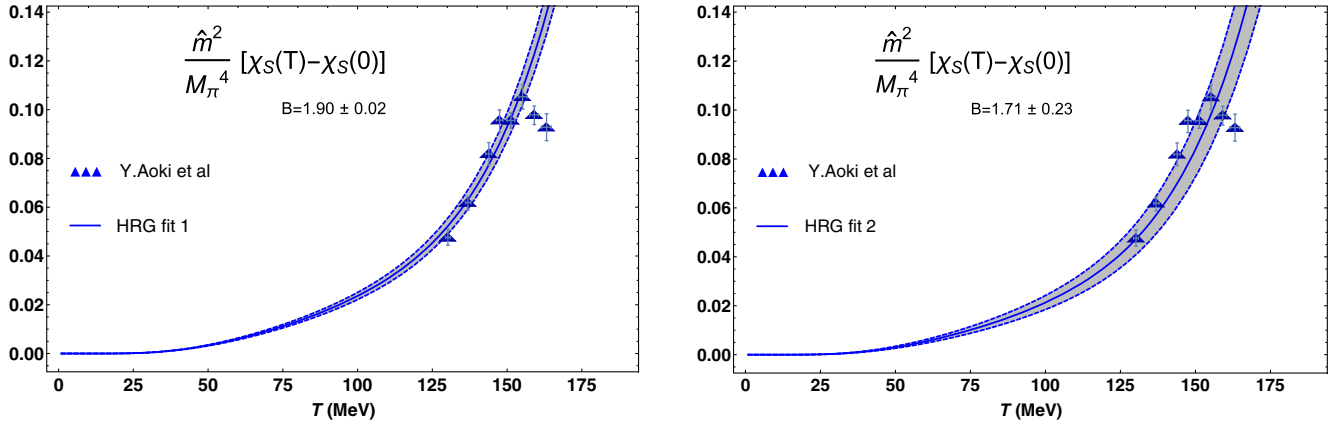

FIG. 8. Fits of the HRG scalar susceptibility with the normalization constant as fit parameter. Fit 1 corresponds to fitting data up to $T \leq T_c = 155$ MeV, while in fit 2, we include two more lattice points, up to $T = 163$ MeV. The quoted uncertainties in the B parameter and the bands correspond to the 95% confidence level of the fit. The lattice data and errors are from Ref. [1].

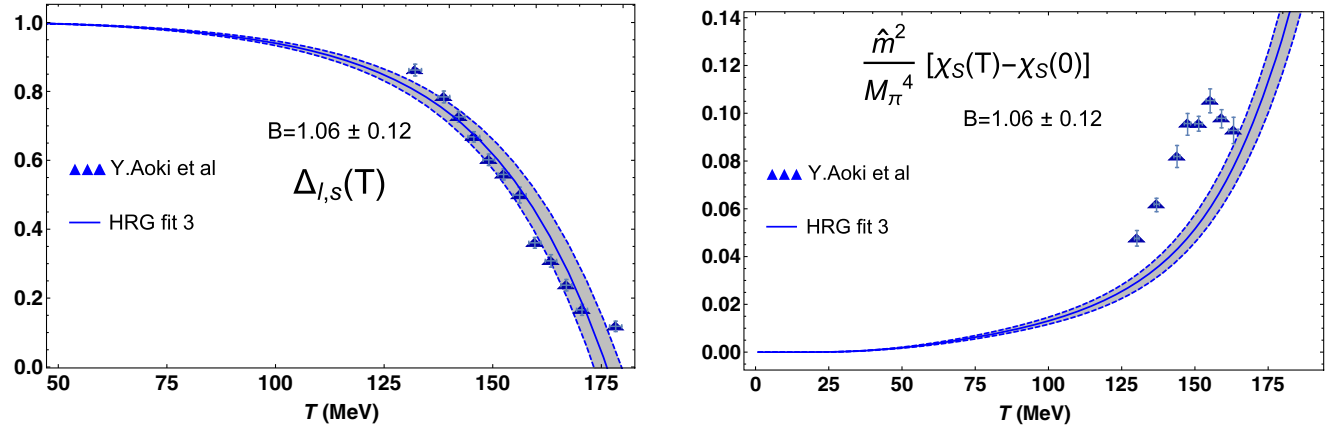

FIG. 9. Left: fit of the HRG reduced condensate with the normalization constant as fit parameter, fitting data up to $T \leq T_c = 155$ MeV. The quoted uncertainties in the B parameter and the bands correspond to the 95% confidence level of the fit. The lattice data and errors are from Ref. [1]. Right: prediction for the scalar susceptibility with the same B central value and uncertainty.

which is one of the condensate combinations for which lattice analysis yield definite predictions, being free of finite-size divergences [1–4]. We include the fitting B parameter as explained before (recall that B multiplies only the finite-temperature correction of quark condensates, not their $T = 0$ part). The result of such a fit (HRG fit 3) is provided in Fig. 9, the fit parameters being given in Table II, and shows a very good description of the reduced condensate, with a value of B compatible with unity and therefore in agreement with the analysis in Ref. [15]. However, that value is incompatible with that in fit 2, i.e., the HRG scalar susceptibility fit in the same temperature range. Such incompatibility is clearly seen in the prediction for χ_S shown in the right panel of that figure. Recall that those lattice data for both quantities come exactly from the same collaboration and lattice setup. The previous claim is confirmed if we try to fit jointly the reduced condensate and scalar susceptibility lattice points. In that case, we obtain a $\chi^2/\mathrm{dof} \simeq 71$, indicating clearly that such a joint description of both quantities within the HRG approach is not feasible.

We could, of course, perform more elaborated fits, such as considering the LECs in the thermal $f_0(500)$ or the hadron masses and their quark mass dependence in the HRG as additional fit parameters. However, the main objective of our present analysis is to compare both approaches and show that actually the thermal $f_0(500)$ one is competitive with respect to the HRG around the transition, and a simple one-parameter fit is enough for such purposes.

V. CONCLUSIONS

In this work, we have performed a detailed analysis of the importance of the thermal corrections to the $f_0(500)$ resonance spectral parameters, regarding the description of the scalar susceptibility χ_S around the region of chiral

symmetry restoration. Such an analysis has been carried out for different realizations of the thermal $f_0(500)$ state within effective theories. First, using the LSM as a test bed, we have shown that a direct relation can be established between the scalar susceptibility and the propagator of the lightest scalar state at zero momentum. Through the analysis of the LSM one-loop σ self-energy at finite temperature, we have shown that the susceptibility saturated by the σ propagator has a much larger growth than the purely perturbative one, approaching better lattice data, although with a divergent behavior in the massive case. The LSM analysis provides additional support for the formulation of χ_S through the UChPT saturated approach, in which the $f_0(500)$ arises as a resonance in $\pi\pi$ scattering, including thermal corrections. The UChPT approach provides a much more reliable description of the $T = 0$ $f_0(500)$ pole and of $\chi_S(T)$ as long as the basic requirements of unitarity and analiticity are maintained. Within the IAM formulation, such an approach actually reproduces correctly the crossover peak and lattice data within the sensitivity of the ChPT low-energy constants. The requirements of unitarity, analiticity, and a good determination of the $T = 0$ pole are crucial to achieve the expected qualitative behavior for the thermal scalar mass, although a correct description of the saturated susceptibility is achieved when the full $\mathcal{O}(p^4)$ corrections to the thermal amplitude are taken into account.

A conclusion shared by the LSM and UChPT approaches is that a saturated approach for $\chi_S(T)$ in which only this thermal state is included can account for most of the lattice data below and even around the transition. For that reason, we have performed several fits of the UChPT saturated approach, with a single parameter fit (normalization factor) comparing it with a description based on the hadron resonance gas in which all hadron states below 2 GeV have been included. The HRG result for $\chi_S(T)$, which had not been analyzed before, provides a better fit than UChPT for temperatures below the transition. However, as values closer to T_c are included, the UChPT improves over the HRG, since it can describe the susceptibility peak. In addition, the HRG fits for the scalar susceptibility are in conflict with those of the quark condensate, using a single-parameter fit.

Through the various approaches analyzed in this work, we conclude that the thermal $f_0(500)$ state is crucial to describe correctly the scalar susceptibility and hence to understand correctly the chiral restoration transition. We believe that our results can be useful in that sense, and we leave for future work related problems such as the possibility to include thermal interactions for the scalar channel within the HRG, which could help us understand previous studies regarding the role of the $f_0(500)$ in that approach.

ACKNOWLEDGMENTS

We are very grateful to J. Ruiz de Elvira and J. Sanz-Cillero for useful comments and discussions. Work partially supported by research Contract No. FPA2016-75654-C2-2-P (Spanish "Ministerio de Economía y Competitividad").

[1] Y. Aoki, S. Borsanyi, S. Durr, Z. Fodor, S. D. Katz, S. Krieg, and K. K. Szabo, J. High Energy Phys. 06 (2009) 088.
[2] S. Borsanyi, Z. Fodor, C. Hoelbling, S. D. Katz, S. Krieg, C. Ratti, and K. K. Szabó (Wuppertal-Budapest Collaboration), J. High Energy Phys. 09 (2010) 073.
[3] A. Bazavov, T. Bhattacharya, M. Cheng, C. DeTar, H. T. Ding, S. Gottlieb, R. Gupta, and P. Hegde *et al.*, Phys. Rev. D **85**, 054503 (2012).
[4] M. I. Buchoff, M. Cheng, N. H. Christ, H.-T. Ding, C. Jung, F. Karsch, Z. Lin, and R. D. Mawhinney *et al.*, Phys. Rev. D **89**, 054514 (2014).
[5] R. D. Pisarski and F. Wilczek, Phys. Rev. D **29**, 338 (1984).
[6] A. V. Smilga and J. J. M. Verbaarschot, Phys. Rev. D **54**, 1087 (1996).
[7] S. Ejiri, F. Karsch, E. Laermann, C. Miao, S. Mukherjee, P. Petreczky, C. Schmidt, W. Soeldner, and W. Unger, Phys. Rev. D **80**, 094505 (2009).
[8] R. Hagedorn, Nuovo Cimento A **56**, 1027 (1968).
[9] F. Karsch, K. Redlich, and A. Tawfik, Phys. Lett. B **571**, 67 (2003).
[10] F. Karsch, K. Redlich, and A. Tawfik, Eur. Phys. J. C **29**, 549 (2003).
[11] A. Tawfik and D. Toublan, Phys. Lett. B **623**, 48 (2005).
[12] S. Leupold, J. Phys. G **32**, 2199 (2006).
[13] P. Huovinen and P. Petreczky, Nucl. Phys. **A837**, 26 (2010).
[14] E. Megias, E. Ruiz Arriola, and L. L. Salcedo, Phys. Rev. Lett. **109**, 151601 (2012).
[15] J. Jankowski, D. Blaschke, and M. Spalinski, Phys. Rev. D **87**, 105018 (2013).
[16] M. Tanabashi *et al.* (Particle Data Group), Phys. Rev. D **98**, 030001 (2018).
[17] P. Gerber and H. Leutwyler, Nucl. Phys. **B321**, 387 (1989).
[18] A. Gomez Nicola, J. R. Pelaez, and J. Ruiz de Elvira, Phys. Rev. D **87**, 016001 (2013).
[19] A. Gomez Nicola, F. J. Llanes-Estrada, and J. R. Pelaez, Phys. Lett. B **550**, 55 (2002).
[20] A. Dobado, A. Gomez Nicola, F. J. Llanes-Estrada, and J. R. Pelaez, Phys. Rev. C **66**, 055201 (2002).
[21] A. Gomez Nicola, F. J. Llanes-Estrada, and J. R. Pelaez, Phys. Lett. B **606**, 351 (2005).

[22] A. Gómez Nicola, J. Ruiz de Elvira, and R. Torres Andres, Phys. Rev. D **88**, 076007 (2013).
[23] J. R. Pelaez, Phys. Rep. **658**, 1 (2016).
[24] M. Gell-Mann and M. Levy, Nuovo Cimento **16**, 705 (1960).
[25] A. Bochkarev and J. I. Kapusta, Phys. Rev. D **54**, 4066 (1996).
[26] A. Ayala and S. Sahu, Phys. Rev. D **62**, 056007 (2000).
[27] J. Gasser and H. Leutwyler, Ann. Phys. (N.Y.) **158**, 142 (1984).
[28] G. Leibbrandt, Rev. Mod. Phys. **47**, 849 (1975).
[29] J. I. Kapusta and C. Gale, *Finite temperature field theory. Principles and Applications* (Cambridge University Press, Cambridge, England, 2006).
[30] T. Hatsuda and T. Kunihiro, Phys. Rev. Lett. **55**, 158 (1985).
[31] V. Bernard, U. G. Meissner, and I. Zahed, Phys. Rev. Lett. **59**, 966 (1987); V. Bernard and U. G. Meissner, Phys. Rev. D **38**, 1551 (1988).
[32] B. Krippa, Nucl. Phys. **A672**, 270 (2000).
[33] D. J. Broadhurst, Nucl. Phys. **B85**, 189 (1975).
[34] M. Bochicchio, L. Maiani, G. Martinelli, G. Rossi, and M. Testa, Nucl. Phys. **B262**, 331 (1985).
[35] A. Gómez Nicola and J. Ruiz de Elvira, J. High Energy Phys. 03 (2016) 186.
[36] A. Gómez Nicola and R. Torres Andrés, Phys. Rev. D **89**, 116009 (2014).
[37] A. V. Manohar and V. Mateu, Phys. Rev. D **77**, 094019 (2008).
[38] P. Masjuan, J. J. Sanz-Cillero, and J. Virto, Phys. Lett. B **668**, 14 (2008).
[39] T. N. Truong, Phys. Rev. Lett. **61**, 2526 (1988); A. Dobado, M. J. Herrero, and T. N. Truong, Phys. Lett. B **235**, 134 (1990); A. Dobado and J. R. Pelaez, Phys. Rev. D **56**, 3057 (1997).
[40] S. Cortés, A. Gómez Nicola, and J. Morales, Phys. Rev. D **93**, 036001 (2016).
[41] C. Hanhart, J. R. Pelaez, and G. Rios, Phys. Rev. Lett. **100**, 152001 (2008).
[42] R. L. Delgado, A. Dobado, and F. J. Llanes-Estrada, Phys. Rev. D **91**, 075017 (2015).
[43] J. A. Oller and E. Oset, Nucl. Phys. **A620**, 438 (1997); **A652**, 407(E) (1999).
[44] A. Schenk, Phys. Rev. D **47**, 5138 (1993).
[45] W. Broniowski, F. Giacosa, and V. Begun, Phys. Rev. C **92**, 034905 (2015).
[46] A. Andronic, P. Braun-Munzinger, and J. Stachel, Nucl. Phys. **A772**, 167 (2006).
[47] A. Andronic, P. Braun-Munzinger, and J. Stachel, Phys. Lett. B **673**, 142 (2009); **678**, 516(E) (2009).
[48] M. Floris, Nucl. Phys. **A931**, 103 (2014).
[49] A. Andronic, P. Braun-Munzinger, K. Redlich, and J. Stachel, Nature (London) **561**, 321 (2018).
[50] X. Luo and N. Xu, J. Nucl. Sci. Technol. **28**, 112 (2017).
[51] A. Gomez Nicola and J. Ruiz de Elvira, Phys. Rev. D **97**, 074016 (2018).
[52] J. Gasser and H. Leutwyler, Nucl. Phys. **B250**, 465 (1985).
[53] D. Blaschke, P. Costa, and Y. L. Kalinovsky, Phys. Rev. D **85**, 034005 (2012).